



# Study of fracture processes in sandstone subjected to four-point bending by means of 4D X-ray computed micro-tomography

Leona Vavro<sup>1</sup>, Martin Vavro<sup>1</sup>, Kamil Souček<sup>1</sup>, Tomáš Fíla<sup>2</sup>, Petr Koudelka<sup>2</sup>, Daniel Vavřík<sup>2</sup>, Daniel Kytýř<sup>2</sup>

<sup>1</sup> The Czech Academy of Sciences, Institute of Geonics, Studentská 1768/9, 708 00 Ostrava-Poruba, Czech Republic

<sup>2</sup> The Czech Academy of Sciences, Institute of Theoretical and Applied Mechanics, Prosecká 809/76, 190 00 Praha 9, Czech Republic

## ABSTRACT

High-resolution X-ray computed micro-tomography (CT) is a powerful technique for studying the processes of crack propagation in non-homogenous quasi-brittle materials such as rocks. To obtain all the significant information about the deformation behaviour and fracture characteristics of the studied rocks, the use of a highly specialised loading device suitable for the integration into existing tomographic setups is crucial. Since no adequate commercial solution is currently available, a completely newly-designed loading device with a four-point bending setup and vertically-oriented scanned samples was used. This design of the loading procedure, coupled with the high stiffness of the loading frame, allows the loading process to be interrupted at any time and for CT scanning to be performed without the risk of the sudden destruction of the scanned sample.

This article deals with the use of the 4D CT for the visualisation of crack initiation and propagation in clastic sedimentary rocks. Two types of quartz-rich sandstones of Czech provenance were used for tomographic observations during the four-point bending loading performed on chevron notched test specimens. It was found that the crack begins to propagate from the moment that ca. 80 % of the maximum loading force is applied.

**Section:** RESEARCH PAPER

**Keywords:** Four-point bending test; chevron-notched core specimen; crack propagation; 4D micro-CT; sandstone

**Citation:** Leona Vavro, Martin Vavro, Kamil Souček, Tomáš Fíla, Petr Koudelka, Daniel Vavřík, Daniel Kytýř, Study of fracture processes in sandstone subjected to four-point bending by means of 4D X-ray computed micro-tomography, Acta IMEKO, vol. 11, no. 2, article 34, June 2022, identifier: IMEKO-ACTA-11 (2022)-02-34

**Section Editor:** Francesco Lamonaca, University of Calabria, Italy

**Received** December 21, 2021; **In final form** March 16, 2022; **Published** June 2022

**Copyright:** This is an open-access article distributed under the terms of the Creative Commons Attribution 3.0 License, which permits unrestricted use, distribution, and reproduction in any medium, provided the original author and source are credited.

**Funding:** This work was supported by the project for the long-term strategic development of research organisations (RVO: 68145535) and the Operational Programme Research, Development, and Education in project INAFYM (CZ.02.1.01/0.0/0.0/16/019/0000766).

**Corresponding author:** Martin Vavro, e-mail: [martin.vavro@ugn.cas.cz](mailto:martin.vavro@ugn.cas.cz)

## 1. INTRODUCTION

The process of crack propagation in quasi-brittle materials due to mechanical loading leading to material failure have been intensively studied by researchers in various disciplines for a very long time. The monitoring of crack initiation and propagation is also of a great importance in rock engineering. The presence of micro- as well as macrocracks significantly influences the strength, deformation, and filtration properties of the rock mass and therefore, strongly affect, for example, the stability of underground workings, tunnels, or open pit slopes. Rock fracture mechanics can also be applied in the prediction of anomalous geomechanical phenomena such as rock bursts or rock and gas

outbursts, or in the evaluation of rock fragmentation processes such as drilling, blasting, crushing, and cutting [1], [2]. More recently, the knowledge about rock fracture processes has been of crucial importance when assessing the suitability of the rock host environment for such demanding engineering applications as CO<sub>2</sub> sequestration or the geological disposal of high-level radioactive waste.

The failure process of rocks and similar rock-like materials is the result of complex mechanisms, including microcrack initiation, propagation, and interactions with each other, resulting in crack coalescence. Eventually, a macroscopic failure plane is generated, thus causing final rock rupture [3], [4]. Cracks in rocks initiate and propagate in response to the applied stress, with the crack path often being driven by the local distribution

of micro-flaws such as cavities, inclusions, fossils, grain boundaries, mineral cleavage planes, and micro-cracks inside the rock [5], [6].

Crack initiation occurs when the stress intensity factor ( $K$ ) at a microcrack tip reaches its critical value, known as the fracture toughness ( $K_c$ ). Fracture toughness thus expresses the resistance of a material to crack initiation and subsequent propagation and represents one of the most important material properties in linear elastic fracture mechanics (LEFM). However, it is important to highlight that rocks and similar geomaterials such as concrete exhibit quasi-brittle behaviour (see [7], [8]), which is typical through the large plastic zone, referred to as the fracture process zone (FPZ), ahead of the crack tip where more complex non-linear fracture processes occur. Due to the FPZ, classical LEFM is not fully applicable for studies related to rock/concrete fracture processes. Thus, the description of fractures needs to be carried out based on non-linear fracture models involving the cohesive nature of the crack propagation; often the fracture energy and/or other softening parameters are utilised [9].

To date, many advanced techniques such as scanning electron microscopy [10], [11] or acoustic emission detection [12], [13] have been adopted to study the progressive failure process of rocks. In the case of these experimental approaches, basic data about crack propagation can be obtained, but the spatial information about deformation processes and FPZ development throughout the tested sample volume remains unknown. For this reason, a wide range of uses is opening up for X-ray CT in the study of the deformation behaviour and fracture processes in rocks.

In this paper, a completely newly designed loading device with a four-point bending setup for vertically oriented scanned samples allowing 4D CT measurements of cracks and FPZ propagation in quasi-brittle materials was used. More specifically, the presented contribution deals with the identification of crack initiation and propagation in two types of Upper Cretaceous quartz sandstones. Both rocks represent well-known building, sculpture, and decorative stone materials that have been used on the Czech territory for many centuries [14].

## 2. ROCK MATERIAL USED FOR THE EXPERIMENTS

Two different types of Czech sandstones, namely the Mšené sandstone and Kocbeře sandstone, were used in the fracture experiments.

The fine-grained Mšené sandstone is almost entirely (> 90 vol. %) composed of quartz grains with an average grain size of 0.15 mm. Other clastic components consist of quartzite, feldspars, and mica flakes. The rock matrix (ca. 5 vol. %) is formed by kaolinite with very finely dispersed Fe-oxyhydroxides (limonite). The degree of secondary silicification is very low.

The fine- to medium-grained Kocbeře sandstone has a bimodal grain size distribution and mainly consists of monocrystalline quartz grains with an average grain size of

0.24 mm and a maximum grain size of 1.5 mm. Quartzite and orthoclase grains occur in a considerably smaller quantity. The matrix and rock cement (10 – 15 vol. %) are formed by quartz which predominates over clay matter. Secondary silicification is intense.

Both sandstones used in the experiments are similar in their mineralogical composition of detrital rock particles but differ in some inner rock texture features as well as in their mineralogical composition of interstitial material between the framework grains. These differences are reflected in different values of physical and mechanical properties (Table 1).

## 3. EXPERIMENTAL SETUP AND INSTRUMENTATION

### 3.1. X-ray CT imaging device

The XT H 225 ST industrial X-ray micro-CT system by Nikon Metrology NV was used to assess the development of the fracture process in fracture toughness tests using chevron bend (CB) test specimens. This X-ray CT scanner is a fully automated apparatus with a rotating scanning system equipped with a micro-focus X-ray source, which generates cone-shaped beams. It is equipped with an X-ray flat panel detector having a number of  $2,000 \times 2,000$  pixels with a pixel size of 200  $\mu\text{m}$ . The basic technical parameters of the XT H 225 ST inspection machine are given, for example, in [17]. The scanning parameters were as follows: a reflection target, 160 kV voltage, 126  $\mu\text{A}$  current, 0.5 mm thick aluminium filter, 3,141 projections with two images per projection, 1,000 ms exposition, a scanning time of ca. 2 hours, and a cubic voxel size of 16  $\mu\text{m}$ . The CT data generated by the micro-scanner were reconstructed using the CT Pro 3D software (Nikon Metrology NV). The visualisation and analysis software VGStudio MAX 3.3 (Volume Graphics GmbH, Germany) was used for data post-processing.

### 3.2. Loading device

Previous research [17], [18] has focussed on the study of the crack propagation processes in quasi-brittle materials, such as silica-based composites or sandstones; these have shown some limitations when the conventional three-point bending tests were used in combination with the X-ray CT technique. The main disadvantage of such an arrangement of the experiment can be seen in particular in the horizontal orientation of the sample perpendicular to the rotational axis of the CT scanner, which, together with the loading supports covering parts of the radiograms (see Figure 1A) significantly reduces the quality of the acquired data.

These shortcomings of the foregoing technical solution have been eliminated with the use of a unique four-point bending loading device which was developed (Czech national patent CZ 307897) at the Institute of Theoretical and Applied Mechanics of the Czech Academy of Sciences in Prague (ITAM CAS). Contrary to the standard arrangement of the three- or four-point

Table 1. Basic physical and mechanical properties of Mšené and Kocbeře sandstones according to various authors (data adopted from [14]-[16]).

Parameter	Mšené sanstone	Kocbeře sandstone
Specific (real) density in $\text{kg}/\text{m}^3$	2,620–2,650	2,630–2,670
Bulk (apparent) density in $\text{kg}/\text{m}^3$	1,850–1,930	2,140–2,490
Total porosity in %	26.3–29.7	12.0–15.3
Water absorption capacity by weight in %	10.8–13.3	2.2–6.1
Uniaxial compressive strength (dry sample) in MPa	21–33	56–87
Flexural strength (dry sample) in MPa	0.9–1.9	5.9–7.9

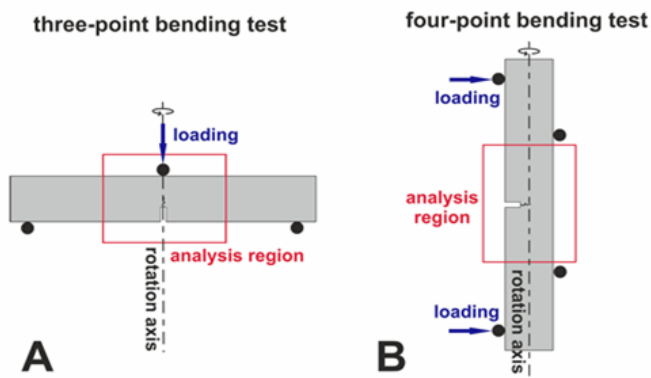


Figure 1. Principal differences between a conventional three-point bending loading scenario (A) and the new four-point bending test with a vertical orientation of the investigated specimen (B).

bending tests using horizontally oriented samples, this novel approach is based on the vertical orientation of the investigated cylindrical specimen, the direction of whose longitudinal axis is identical to that of the rotational axis of the CT scanner (Figure 1B). This concept significantly reduces differences in the attenuation of X-rays observed during the rotation of the sample subjected to a CT scan.

The modular device for four-point bending during micro-CT sequences consists of three main components. A pair of motorised movable supports are integrated with driving units with precision captive stepper linear actuators (23-2210, Koco Motion DINGS, USA) and precision linear guideways (MGW12, Hiwin, Japan). The driving units are equipped with linear encoders (LM10, Renishaw Inc., United Kingdom) ensuring positioning with 1  $\mu\text{m}$  resolution and load cells (LCM300, Futek, USA) with nominal capacity 1,250 N. The central part of the device frame exposed to X-ray beam is manufactured from a carbon fiber composite (MTM57 series epoxy resin, T700S carbon fibers, shell nominal thickness 1.95 mm) providing

sufficient frame stiffness and low attenuation of X-rays. Cylindrical load-bearing frame, housing the loaded specimen, together with all the components of the loading device are manufactured from high strength aluminium alloy (EN-AW-6086-T6). The small distance between the X-ray source and the scanned objects also allows for the high resolution of the reconstructed 3D images, which is necessary for a detailed tomographic investigation of the loaded sample. The high stiffness of the loading frame and high precision control of the loading force during the experiment allow for the subsequent interruption of the loading process at any point of both the ascending and descending parts of the rock's load-displacement (F-d) curve without the risk of sudden sample collapse. A more detailed technical description of the in-house four-point measuring device is provided in [19]. The device and its scheme are shown in partial section in Figure 2A.

### 3.3. Test specimens and experimental procedure

Cylindrical CB specimens with a diameter of 29 mm and a length of approximately 195 mm were drilled from sandstone blocks in the laboratory. The core drilling was carried out parallel to the sandstone bedding planes. In the central part of the test specimen, a chevron edge notch was carved using a circular diamond blade. The width of the chevron notch was 1.4 mm.

A prepared cylindrical specimen was inserted into the specimen chamber placed into the X-ray CT inspection system (Figure 2B) and centred inside this chamber on the supports. The orientation of the longitudinal axis of the specimen, emplaced in the test-ready position, was identical to that of the rotational axis of the loading device. After the initial contact of the specimen with the loading parts, its stable position was secured by applying a contact force of 5 N. Then, the inspection using transmission radiography was performed to verify the correct position of the chevron notch tip and to exclude the samples with significant inhomogeneity in the volume of interest in the vicinity of the notch. Pre-peak loading was performed in force control mode by prescribing its linear increase and ensuring a uniform load

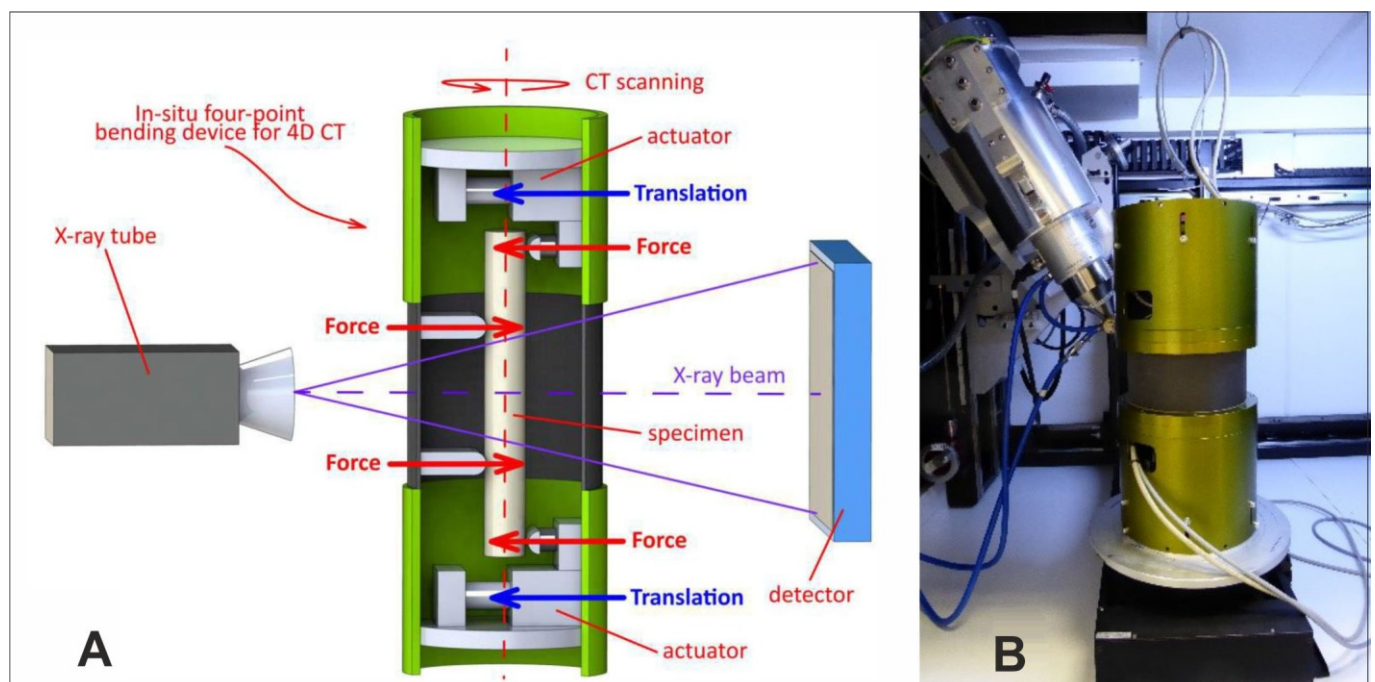


Figure 2. Four-point loading device for 4D micro-CT experiments: (A) longitudinal cross-section of the loading device, (B) loading device attached to the rotation table of the XT H 225 ST X-ray micro-CT scanner.

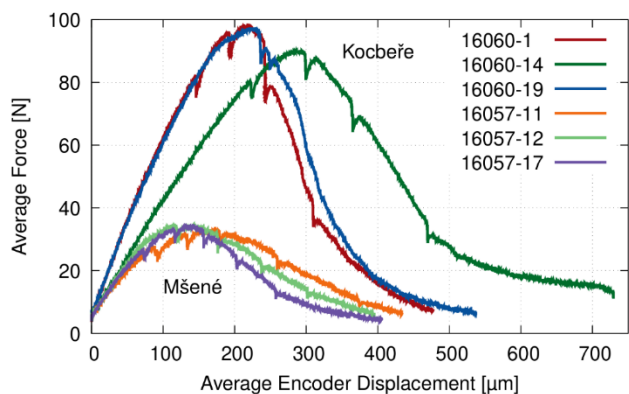


Figure 3. Loading curves of Mšené (sample no. 16057) and Kocbeře (sample no. 16060) sandstones with well visible loading gaps observed by CT scanning. The  $F$ - $d$  diagram of the individual rock sample 16057/11 from the Mšené sandstone is presented in detail in Figure 4.

distribution on the supports (outer supports span  $L_{out} = 179$  mm, inner supports span  $L_{in} = 75$  mm). Post-peak loading was performed in displacement control mode with a position increment identical for both loading supports to prevent the sudden rupture of the specimen caused by the eventual non-symmetrical response of the specimen. During the loading procedure, the test time, the displacement value, and the loading force were recorded continuously, with the sampling frequency of the displacements and the load of the external support being 200 Hz using an in-house developed control software [20].

During the experiment, the loading process was interrupted at four to five loading steps, where imaging via X-ray micro-CT

scanner was carried out. In the loading sequence, one or two load-steps were performed during the rock's hardening phase, one load-step near the ultimate-stress point, and two or three load-steps were performed during the post-peak softening phase, without the sudden cracking of the specimen. The maximal loading force reached approximately 30 N to 35 N in the case of Mšené sandstone and between 90 N and 100 N when the Kocbeře sandstone was tested (Figure 3). The force drops in the recorded loading diagrams were caused by material relaxation during the time-lapse tomography scanning. It is also clear from Figure 3 that three test specimens were examined for each of the two above mentioned sandstone types. One of them, namely specimen 16057/11 from the Mšené sandstone, was then selected for a detailed description of the process of crack propagation, which is presented in Section 4.

#### 4. RESULTS

The measured data acquired from the loading device were subsequently processed in the form of  $F$ - $d$  diagrams. In Figure 4, the displacement-load curve of one selected test sample is shown.

As can be seen from Figure 4, a total of six micro-CT measurements were taken at points A to F while loading sample 16057/11. A reference CT measurement (scan A) was realised immediately after the fixation of the rock specimen in the loading device, at a minimal loading of 5 N. Two other consecutive measurements were performed at points B and C before reaching the maximum load, i.e., in the ascending portion of the load-displacement plot. Specifically, measurement B was made at a loading level of 26 N (i.e., at ca. 80% of the maximal force) and

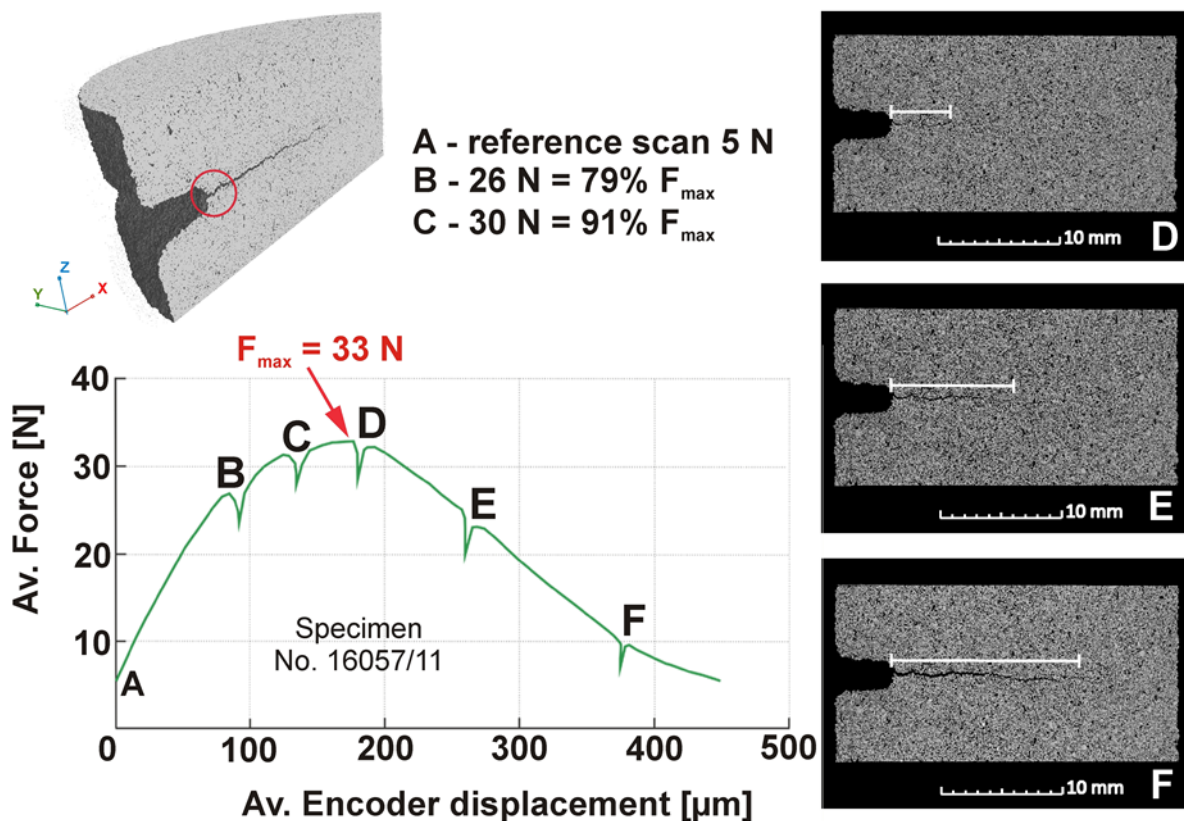


Figure 4.  $F$ - $d$  diagram of a selected rock sample prepared from the Mšené sandstone (16057/11) with CT slices obtained at different loading steps (D, E, and F) on the descending part of the loading curve. A macroscopically visible crack path is highlighted by white lines. The red circle in the vertical cross-section of the loaded specimen (upper left corner) defines the area, which is in the case of loading steps A, B, and C zoomed in onto and presented in Figure 5.

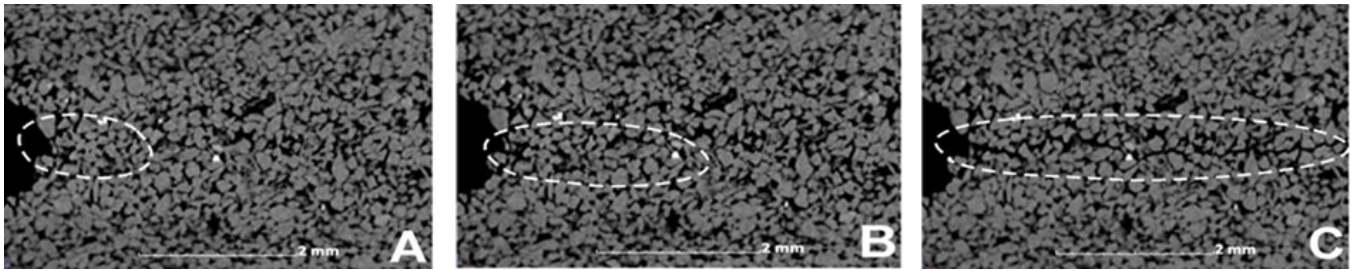


Figure 5. Series of zoomed CT images of a selected Mšene sandstone rock sample (16057/11) acquired at the different loading steps (A, B, and C) on the ascending part of the F-d loading curve. The changes in sandstone microtexture related to crack origin are highlighted by white ellipses.

measurement C at a loading of 30 N, which corresponded to about 90 % of the peak force. Measurement D practically corresponded to the ultimate stress point. The last two measurements, E and F, were made during the post-peak phase, at loads of 24 N and 9 N, respectively. The presented measurements clearly showed that even such low-strength rock samples, where the peak force reached only 33 N, can be successfully subjected to loading with discrete steps during strain softening without the risk of their sudden collapse.

The process of crack propagation during the post-peak behaviour is well visible in the CT images presented in Figure 4. Generally, it is assumed that the real crack begins to propagate when the load reaches the ultimate stress point (see e.g., [21]). However, based on previous experience acquired during radiographic measurements in a three-point bending loading scenario [17], our current research was focussed mainly on the identification of the possible manifestation of crack origins and their subsequent growth on the ascending part of the loading curve.

As for the pre-peak crack propagation, CT images taken before the load reached the peak value are shown in Figure 5.

This figure indicates that the apparent crack developing from a crack tip was present also within step C, i.e., at a level of ca. 90 % of the maximal loading force ( $F_{max}$ ). When compared to reference step A, some changes were visible in the sandstone microtextures in scan B (ca. 80 % of  $F_{max}$ ) near the crack tip related to crack evolution. These changes are reflected in the movement of individual quartz grains apart from each other. Based on these findings, it can be concluded that, in the case of the studied sandstones, the crack began to propagate from the moment when approximately 80 % of the maximum loading force was applied. However, it should be noted, that the crack path was hard to identify in some parts of the reconstructed CT slices due to heterogenous sandstone microtextures, especially due to the presence of pores. This problem can be overcome by using differential tomography, where changes in the object are emphasised by the differentiation of the actual and the reference tomographic reconstructions, as recently described by e.g., [16] and [19]. The differences between the states at points B and C, respectively, and the initial state (A) are presented in Figure 6.

The development of the crack during mechanical loading was manifested by an increase of open porosity in the area of the

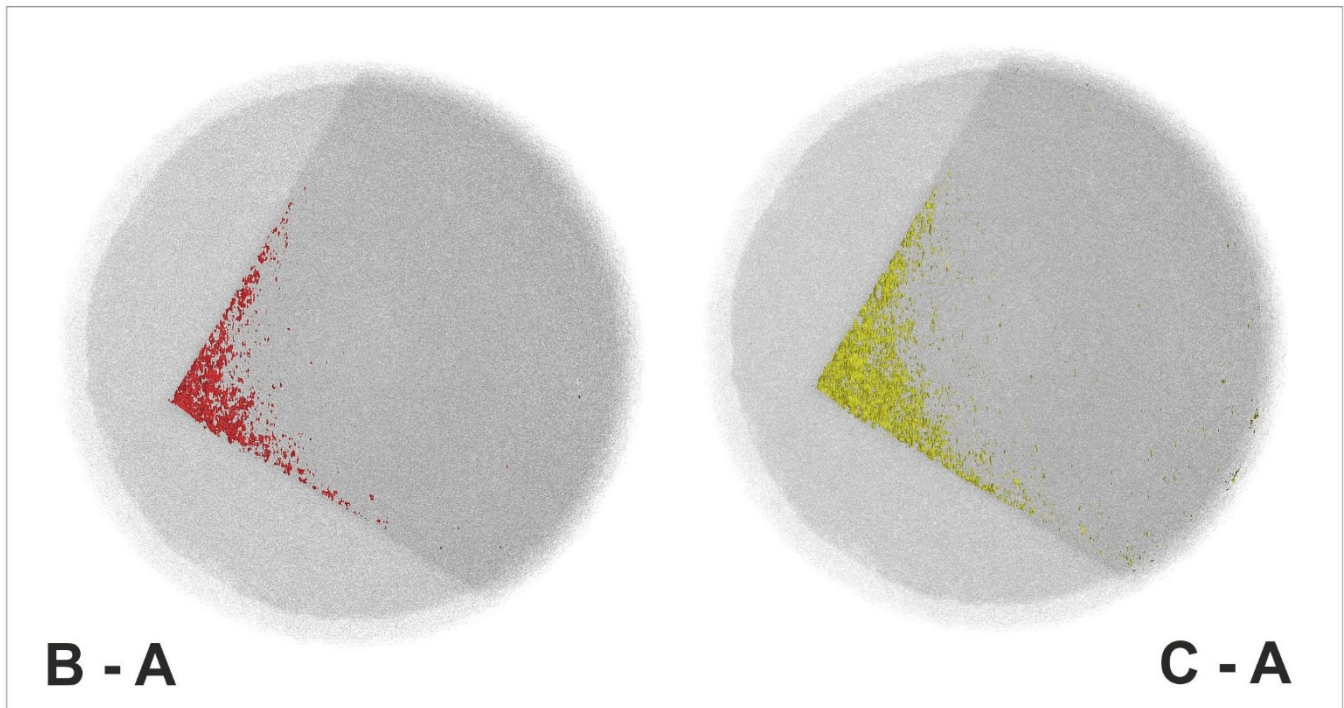


Figure 6. Visualisation of the development of the crack shape in loading steps B and C using tomographic image subtraction between the actual (loaded) and reference (unloaded) states; i.e., the image on the left represents the difference between steps B and A and the one on the right is a subtraction between the C and A loading steps.

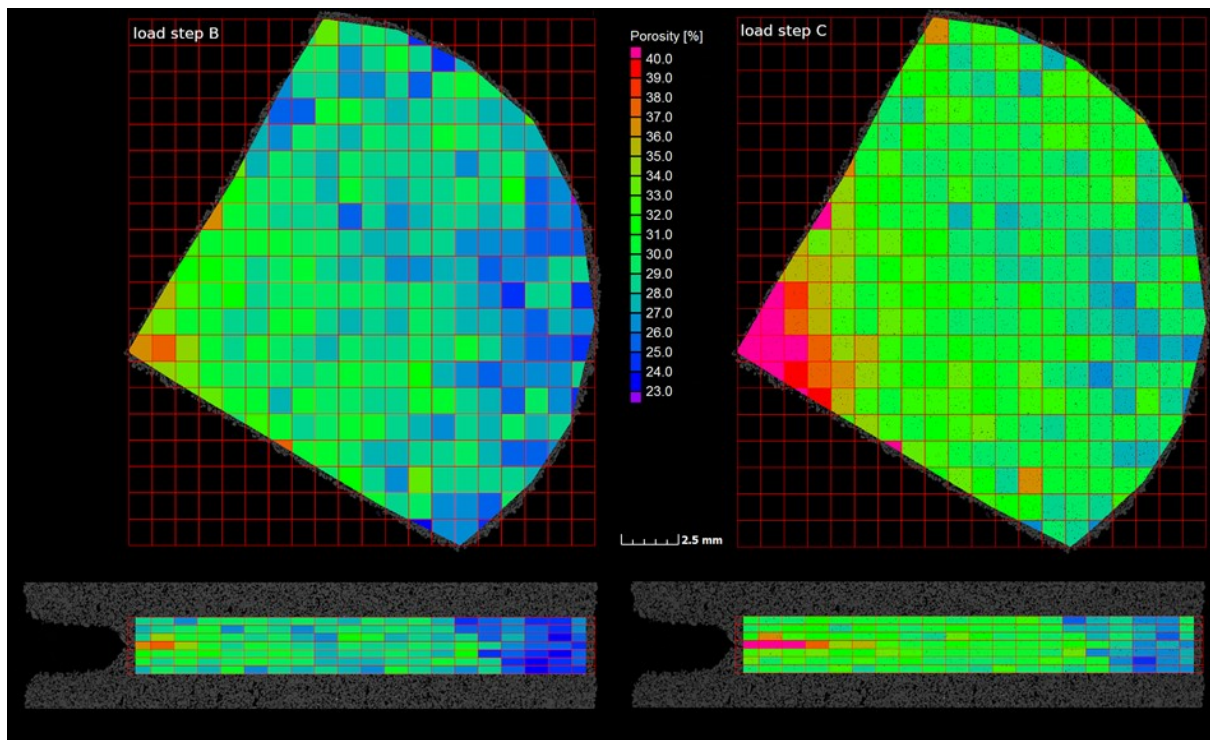


Figure 7. Changes in the distribution of rock porosity in XY (upper images) and XZ (bottom images) planes due to crack development. It should be noted that the open porosity of the intact Mšené sandstone measured by mercury intrusion porosimetry reached values between ca. 26 % and 30 % as reported by e.g., [19], [22], or [23]).

crack spreading through the rock test specimen, which is clearly shown in Figure 7. The figure shows porosity distribution under the tip of the notch in two consecutive loading steps from the tests of the Mšené sandstone test specimen no. 16057/11. Using a hexahedral mesh grid superimposed on the reconstructed 3D images, where the porosity was evaluated in every hexahedral region of interest as an average over its volume, it can be seen that the macroscopic crack developed before the ultimate stress point was reached.

## 5. CONCLUSIONS

The study performed on the rock samples prepared from quartz-rich Mšené and Kocbeře sandstones showed that crack development and propagation can be successfully observed in 3D thanks to the joint use of a four-point bending procedure and high-resolution 4D micro-CT measurements. A four-point bending device that was newly developed at ITAM CAS allows the study of fracture processes in rocks and similar quasi-brittle materials with high precision. The measurements also showed that the concept of vertically oriented rock samples in four-point bending devices for 4D micro-CT provides considerable advantages over the standard horizontally oriented three-point or four-point bending setups.

In the studied sandstones, it was observed that the process of crack propagation starts from the moment when approximately 80% of the maximum loading force is applied. This outcome is in very good agreement with the results of previous research [16], [17], which was performed on the different types of sandstone regarding their microtextural features, mineralogical compositions, and related physical and mechanical properties.

Therefore, this research confirmed the fact that the crack, which was formed and started to propagate before the peak load was reached, was further propagated during the post-peak phase.

More specifically, the crack length at point D (maximal loading force) was approximately 4.9 mm, which increased to 9.8 mm and 15.2 mm at points E and F, respectively. These crack lengths measured for post-peak strain softening phase are very similar to the values which were published by [19] for a stronger variety of Mšené sandstone.

The observation that the process of crack propagation started before reaching the maximum load is consistent with previous knowledge obtained for various types of German, American, or Chinese sandstones by means of digital image correlation [24] or acoustic emission techniques [25]-[28]. Moreover, this finding is also valid for other quasi-brittle materials, such as concrete, as confirmed by the study of AE signals both in flexural [29] and compressive [30] loading modes.

## ACKNOWLEDGEMENT

The presented work was supported by the project for the long-term strategic development of research organisations (RVO: 68145535) and the Operational Programme Research, Development, and Education in project INAFYM (CZ.02.1.01/0.0/0.0/16/019/0000766).

## REFERENCES

- [1] ISRM Commission on Testing Methods (F. Ouchterlony, co-ordinator), Suggested methods for determining the fracture toughness of rock, *Int. J. Rock Mech. Min. Sci. & Geomech. Abst.* 25(2) (1988), pp. 71–96.
- [2] B. N. Whittaker, R. N. Sing, G. Sun, *Rock fracture mechanics: principles, design and applications*, Elsevier Science Publishers B.V., Amsterdam, The Netherlands, 1992, ISBN 978-0444896841.
- [3] H. Haeri, K. Shahriar, M. F. Marji, P. Moarefvand, Experimental and numerical study of crack propagation and coalescence in pre-cracked rock-like disks, *Int. J. Rock Mech. Min. Sci.* 67 (2014), pp. 20–28.

- DOI: [10.1016/j.ijrmms.2014.01.008](https://doi.org/10.1016/j.ijrmms.2014.01.008)
- [4] C. A. Tang, S. Q. Kou, Crack propagation and coalescence in brittle materials under compression, *Eng. Fract. Mech.* 61(3-4) (1998), pp. 311–324.  
DOI: [10.1016/S0013-7944\(98\)00067-8](https://doi.org/10.1016/S0013-7944(98)00067-8)
- [5] S. Zabler, A. Rack, I. Manke, K. Thermann, J. Tiedemann, N. Harthill, H. Riesemeier, High-resolution tomography of cracks, voids and micro-structure in greywacke and limestone. *J. Struct. Geol.* 30(7) (2008), pp. 876–887.  
DOI: [10.1016/j.jsg.2008.03.002](https://doi.org/10.1016/j.jsg.2008.03.002)
- [6] J. B. Zhu, T. Zhou, Z. Y. Liao, L. Sun, X. B. Li, R. Chen, Replication of internal defects and investigation of mechanical and fracture behaviour of rock using 3D printing and 3D numerical methods in combination with X-ray computerized tomography, *Int. J. Rock Mech. Min. Sci.* 106 (2018), pp. 198–212.  
DOI: [10.1016/j.ijrmms.2018.04.022](https://doi.org/10.1016/j.ijrmms.2018.04.022)
- [7] Z. P. Bazant, J. Planas, *Fracture and size effect in concrete and other quasibrittle materials*, 1st edn. CRC Press LLC, Boca Raton (FL), USA, 1998, ISBN 978-0849382840.
- [8] S. P. Shah, S. E. Swartz, C. Ouyang, *Fracture mechanics of structural concrete: applications of fracture mechanics to concrete, rock, and other quasi-brittle materials*. 1st edn. John Wiley & Sons Inc, New York, USA, 1995, ISBN 978-0-471-30311-4.
- [9] L. Vavro, L. Malíková, P. Frantík, P. Kubeš, Z. Keršner, M. Vavro, An advanced assessment of mechanical fracture parameters of sandstones depending on the internal rock texture features, *Acta Geodyn. Geomater.* 16(2) (2019), pp. 157–168.  
DOI: [10.13168/AGG.2019.0013](https://doi.org/10.13168/AGG.2019.0013)
- [10] P. Baud, E. Klein, T. F. Wong TF, Compaction localization in porous sandstones: spatial evolution of damage and acoustic emission activity, *J. Struct. Geol.* 26(4) (2004), pp. 603–624.  
DOI: [10.1016/j.jsg.2003.09.002](https://doi.org/10.1016/j.jsg.2003.09.002)
- [11] Z. Brooks, F. J. Ulm, H. H. Einstein, Environmental scanning electron microscopy (ESEM) and nanoindentation investigation of the crack tip process zone in marble, *Acta Geotech.* 8(3) (2013), pp. 223–245.  
DOI: [10.1007/s11440-013-0213-z](https://doi.org/10.1007/s11440-013-0213-z)
- [12] D. Lockner, J. D. Byerlee, V. Kukusenko, A. Ponomarev, A. Sidorin, Quasi-static fault growth and shear fracture energy in granite, *Nature* 350 (1991), pp. 39–42.  
DOI: [10.1038/350039a0](https://doi.org/10.1038/350039a0)
- [13] E. Townend, B. D. Thompson, P. M. Benson, P. G. Meredith, P. Baud, R. P. Young, Imaging compaction band propagation in Diemelstadt sandstone using acoustic emission locations, *Geophys. Res. Letters* 35(15) (2008), L15301.  
DOI: [10.1029/2008GL034723](https://doi.org/10.1029/2008GL034723)
- [14] V. Rybařík, *Noble building and sculptural stone of the Czech Republic*, Industrial Secondary School of Stonework and Sculpture in Hořice, Hořice, Czech Republic, 1994, ISBN 80-900041-5-6 [in Czech].
- [15] P. Koutník, P. Antoš, P. Hájková, P. Martinec, B. Antošová, P. Ryšánek, J. Pacina, J. Šancer, J. Ščučka, V. Brůna, *Decorative stones of Bohemia, Moravia and Czech Silesia*. Jan Evangelista Purkyně University in Ústí nad Labem, Ústí nad Labem, Czech Republic, 2015, ISBN 978-8074149740 [in Czech].
- [16] D. Vavrik, P. Benes, T. Fila, P. Koudelka, I. Kumpova, D. Kytir, M. Vopalensky, M. Vavro, L. Vavro, Local fracture toughness testing of sandstone based on X-ray tomographic reconstruction, *Int. J. Rock Mech. Min. Sci.* 138 (2021), art. no. 104578.  
DOI: [10.1016/j.ijrmms.2020.104578](https://doi.org/10.1016/j.ijrmms.2020.104578)
- [17] L. Vavro, K. Souček, D. Kytýř, T. Fila, Z. Keršner, M. Vavro, Visualization of the evolution of the fracture process zone by transmission computed radiography, *Procedia Eng.* 191 (2017), pp. 689–696.  
DOI: [10.1016/j.proeng.2017.05.233](https://doi.org/10.1016/j.proeng.2017.05.233)
- [18] I. Kumpová, M. Vopálenký, T. Fila, D. Kytýř, D. Vavřík, M. Pichotka, J. Jakůbek, Z. Keršner, J. Klon, S. Seitl, J. Sobek, On-the-fly fast X-ray tomography using CdTe pixelated detector – Application in mechanical testing, *IEEE Trans. Nucl. Sci.* 65(12) (2018), pp. 2870–2876.  
DOI: [10.1109/TNS.2018.2873830](https://doi.org/10.1109/TNS.2018.2873830)
- [19] P. Koudelka, T. Fila, V. Rada, P. Zlamal, J. Sleichert, M. Vopalensky, I. Kumpova, P. Benes, D. Vavrik, L. Vavro, M. Vavro, M. Drdacky, D. Kytir, In-situ X-ray differential microtomography for investigation of water-weakening in quasi-brittle materials subjected to four-point bending, *Materials* 13(6) (2020), art. no. 1405.  
DOI: [10.3390/ma13061405](https://doi.org/10.3390/ma13061405)
- [20] V. Rada, T. Fila, P. Zlamal, D. Kytir, P. Koudelka, Multi-channel control system for in-situ laboratory loading devices, *Acta Polytech. CTU Proc.* 18 (2018), pp. 15–19.  
DOI: [10.14311/APP.2018.18.0015](https://doi.org/10.14311/APP.2018.18.0015)
- [21] M. D. Wei, F. Dai, N. W. Xu, T. Zhao, Stress intensity factors and fracture process zones of ISRM-suggested chevron notched specimens for mode I fracture toughness testing of rocks, *Eng. Fract. Mech.* 168(A) (2016), pp. 174–189.  
DOI: [10.1016/j.engfracmech.2016.10.004](https://doi.org/10.1016/j.engfracmech.2016.10.004)
- [22] J. Desarnaud, H. Derluyn, L. Molari, S. De Miranda, V. Cnudde, N. Shahidzadeh, Drying of salt contaminated porous media: Effect of primary and secondary nucleation, *J. Appl. Phys.* 118(11) (2015), art. no. 114901.  
DOI: [10.1063/1.4930292](https://doi.org/10.1063/1.4930292)
- [23] Z. Pavlík, P. Michalek, M. Pavlíkova, I. Kopecka, I. Maxova, R. Cerny, Water and salt transport and storage properties of Mšené sandstone, *Constr. Build. Mater.* 22(8) (2008), pp. 1736–1748.  
DOI: [10.1016/j.conbuildmat.2007.05.010](https://doi.org/10.1016/j.conbuildmat.2007.05.010)
- [24] Q. Lin, J. F. Labuz, Fracture of sandstone characterized by digital image correlation, *Int. J. Rock Mech. Min. Sci.* 60 (2013), pp. 235–245.  
DOI: [10.1016/j.ijrmms.2012.12.043](https://doi.org/10.1016/j.ijrmms.2012.12.043)
- [25] T. Backers, S. Stanchits, G. Dresen, Tensile fracture propagation and acoustic emission activity in sandstone: the effect of loading rate, *Int. J. Rock Mech. Min. Sci.* 42(7–8) (2005), pp. 1094–1101.  
DOI: [10.1016/j.ijrmms.2005.05.011](https://doi.org/10.1016/j.ijrmms.2005.05.011)
- [26] W. Li, F. U. A. Shaikh, L. Wang, Y. Lu, K. Wang, Z. Li, Microscopic investigation of rate dependence on three-point notched-tip bending sandstone, *Shock Vib.* (2019), art. no. 4525162.  
DOI: [10.1155/2019/4525162](https://doi.org/10.1155/2019/4525162)
- [27] H. Zhang, D. Fu, H. Song, Y. Kang, G. Huang, G. Qi, J. Li, Damage and fracture investigation of three-point bending notched sandstone beams by DIC and AE techniques, *Rock Mech. Rock Eng.* 48(3) (2015), pp. 1297–1303.  
DOI: [10.1007/s00603-014-0635-4](https://doi.org/10.1007/s00603-014-0635-4)
- [28] W. K. Zietlow, J. F. Labuz, Measurement of the intrinsic process zone in rock using acoustic emission, *Int. J. Rock Mech. Min. Sci.* 35(3) (1998), pp. 291–299.  
DOI: [10.1016/S0148-9062\(97\)00323-9](https://doi.org/10.1016/S0148-9062(97)00323-9)
- [29] J. F. Labuz, S. Cattaneo, L. H. Chen, Acoustic emission at failure in quasi-brittle materials, *Constr. Build. Mater.* 15(5–6) (2001), pp. 225–233.  
DOI: [10.1016/S0950-0618\(00\)00072-6](https://doi.org/10.1016/S0950-0618(00)00072-6)
- [30] D. L. Carnì, C. Scuro, F. Lamonaca, R. S. Olivito, D. Grimaldi, Damage analysis of concrete structures by means of acoustic emissions technique, *Compos. B. Eng.* 115 (2017), pp. 79–86.  
DOI: [10.1016/j.compositesb.2016.10.031](https://doi.org/10.1016/j.compositesb.2016.10.031)